Supporting Information

Lattice Doping of Lanthanide Ions in Cs_2ZrCl_6 Nanocrystals Enabling Phase Transition and Tunable Photoluminescence

Yachong Liu[a,b,c,d], Rui Yun[a,b,c,d], Huanxin Yang[a,b,c,d], Wenda Sun[a,b,c,d], Yue Li[a,b,c,d], Haolin Lu[e], Libing Zhang[f] and Xiyan Li[a,b,c,d*]

[a] *Institute of Photoelectronic Thin Film Devices and Technology of Nankai University, Tianjin 300350, China*

[b] *Tianjin Key Laboratory of Efficient Utilization of Solar Energy, Tianjin 300350, China*

[c] *Research Center of Thin Film Photoelectronic Technology, Ministry of Education, Tianjin 300350, China*

[d] *State Key Laboratory of Photovoltaic Materials and Cells, Tianjin 300350, China*

[e] *Tianjin Key Lab for Rare Earth Materials and Applications, Renewable Energy Conversion and Storage Center, Smart Sensing Interdisciplinary Science Center, School of Materials Science and Engineering, National Institute for Advanced Materials, Nankai University, Tianjin 300350, China*

[f] *Tianjin Key Laboratory of Molecular Optoelectronic Sciences, Department of Chemistry, Tianjin University, Tianjin 300072, China*

[*] *Corresponding author.*

E-mail: xiyan.li@nankai.edu.cn(X. Li).

Experimental Section

Materials. $Tb(CH_3CO_2)_3 \cdot xH_2O$ (99.9%), $Eu(CH_3CO_2)_3 \cdot xH_2O$ (99.9%), $Dy(CH_3CO_2)_3 \cdot xH_2O$ (99.9%), $Sm(CH_3CO_2)_3 \cdot xH_2O$ (99.9%), $Pr(CH_3CO_2)_3 \cdot xH_2O$ (99.9%) were purchased from Heowns. Cesium Acetate (CsOAc, aladdin, 99%), acetic acid (CH_3COOH, ≥99.8%), Trimethylchlorosilane (TMSCl, > 99.0%), Cyclohexane (99.5%), Oleic acid (OA, AR), Oleylamine (OAm, 80%-90%), 1-Octadecene (ODE, 90%) and were purchased from Aladdin. Bismuth acetate ($Bi(CH_3CO_2)_3$, 99.99%) was purchased from HWRK Chem. Zirconium dicarbonate ($Zr(CO_3)_2$, 99.90%) was purchased from Bidepharm. Methyl acetate (99%) was purchased from Macklin. All of raw materials were used as received without further purification.

Physical Measurements. The X-ray diffraction (XRD) results of samples were recored by the Ultima X-ray diffractometer (Rigaku, Japan), with Cu Kα (λ = 1.5405 Å) as the irradiation source under 40 kV–40 mA power, and the scanning rate was set to 10 degrees per minute. The particle images, high-resolution TEM images and elements mapping were measured by the field emission transmission electron microscope (TEM, JEM-2800, Japan) equipped with an energy dispersive spectroscopy (EDS), operated at an acceleration voltage of 200 kV. The photoluminescence spectra (PL), photoluminescence excitation spectra (PLE), photoluminescence quantum yield (PLQY), photoluminescence decay curves were obtained by a FS5 spectrofluorometer (Edinburg, England) equipped with a integrating sphere. The absorption spectra were obtained by a UV-Vis spectrophotometer (UV-2600, Shimadzu, Japan). X-ray photoelectron spectroscopy (XPS) spectra were carried out with an Thermo ESCALAB 250XI X-ray photoelectron spectrometer (America) equipped with an Al Kα source. Unless otherwise specified, all spectra were recorded under identical experimental conditions. Key experiments were repeated three times and other experiments were repeated twice.

Synthesis of undoped Cs_2ZrCl_6 nanocrystals. The undoped Cs_2ZrCl_6 NCs were prepared by an improved hot injection method.[1] First, 1.42 mmol (300 mg) $Zr(CO_3)_2$ white powder was loaded into a three-necked flask containing 10 ml ODE and 325 μL CH_3COOH. Then the mixture was slowly heated to 50°C-60°C for about 5 min. When a clear and transparent solution was formed, 0.709 mmol (136 mg) CsOAc, 2.8 mL oleic acid, and 615 μL oleamine were successively added to the flask. Next the mixture was slowly heated to 108℃, kept in a degassed state during heating, vacuum dried for 1.5 h, and then heated to 200℃ in N_2 atmosphere. After this temperature was reached, 500 μL TMSCl was rapidly injected. After about 20 seconds of reaction, the resulting coarse solution was quickly cooled in an ice water bath. In the washing process, the crude solution, cyclohexane and methyl acetate were first mixed in a ratio of 1:1:2 by volume, then centrifugated at 10000 rpm for 10 min, poured out the light-colored supernatant, redispersed the precipitate into 10 ml cyclohexane, and then centrifugated again at 5000 rpm for 5 min. After centrifugation, the supernatant was collected and sealed for storage at 4℃.

Synthesis of Ln^{3+}-doped Cs_2ZrCl_6 and undoped Cs_3LnCl_6 nanocrystals. $Cs_2Zr_{(1-x)}Cl_6:xLn^{3+}$ NCs and undoped Cs_3LnCl_6 were synthesized by the same method as undoped Cs_2ZrCl_6 NCs with minor modifications.[2] The doping ratios of rare earth ions were following the Ln/(Ln+Zr) precursors ratio of 0, 1%, 2%, 3%, 5%, 8%, 10%, 20%, 40%, 50%, 60%, 100%. First, 1.42x mmol rare-earth acetate powder (x = 0% ~ 100%) and 1.42(1-x) mmol $Zr(CO_3)_2$ white powder were added to the raw material, and other reaction parameters were the same. When x = 100%, undoped Cs_3LnCl_6 NCs were synthesized.

Synthesis of Bi^{3+}-doped Cs_2ZrCl_6 nanocrystals. The synthetic method of the $Cs_2Zr_{80\%}Cl_6:20\%Bi^{3+}$ NCs were identical to that for Ln^{3+}-doped Cs_2ZrCl_6 NCs except for the use of $20\%Bi^{3+}$ ions instread of $20\%Ln^{3+}$ ions.

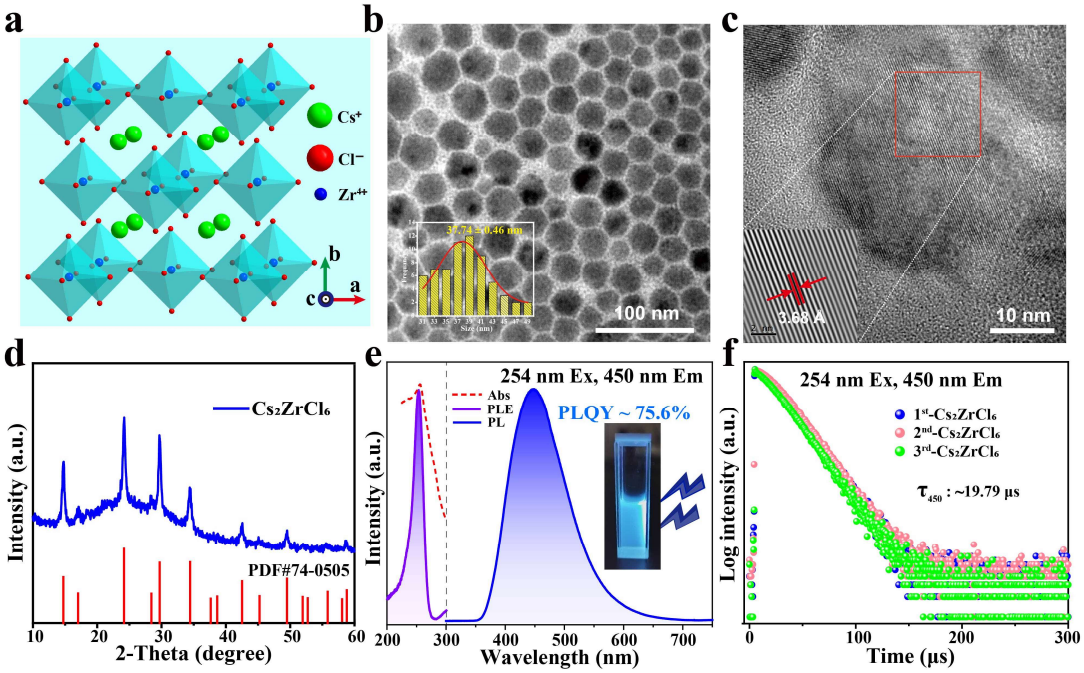

Figure S1. (a) Crystal structure of the Cs_2ZrCl_6 NCs. (b) TEM images and size distributions of Cs_2ZrCl_6 NCs. (c-d) HRTEM images and XRD of Cs_2ZrCl_6 NCs. (e) UV-vis absorption, PLE and PL spectra of Cs_2ZrCl_6 NCs (Ex: Excitation, Em: Emission). (f) PL decay curves of three parallel samples of Cs_2ZrCl_6 NCs at 450 nm.

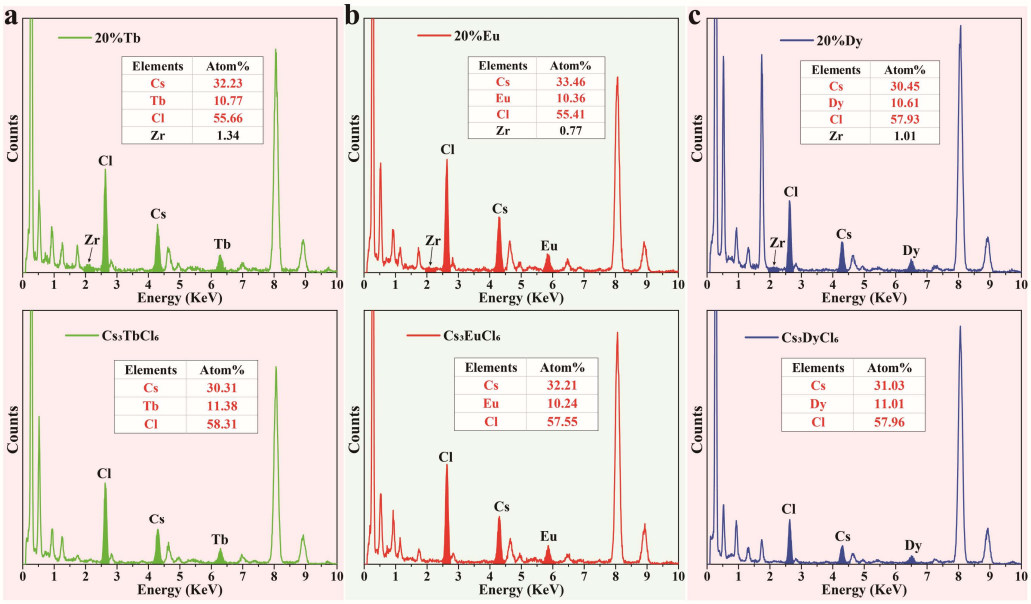

Figure S2. Energy dispersive X-ray (EDX) spectrum for (a) 20%Tb^{3+}-doped Cs_2ZrCl_6 NCs and undoped Cs_3TbCl_6 NCs, (b) 20%Eu^{3+}-doped Cs_2ZrCl_6 NCs and undoped Cs_3EuCl_6 NCs, (c) 20%Dy^{3+}-doped Cs_2ZrCl_6 NCs and undoped Cs_3DyCl_6 NCs.

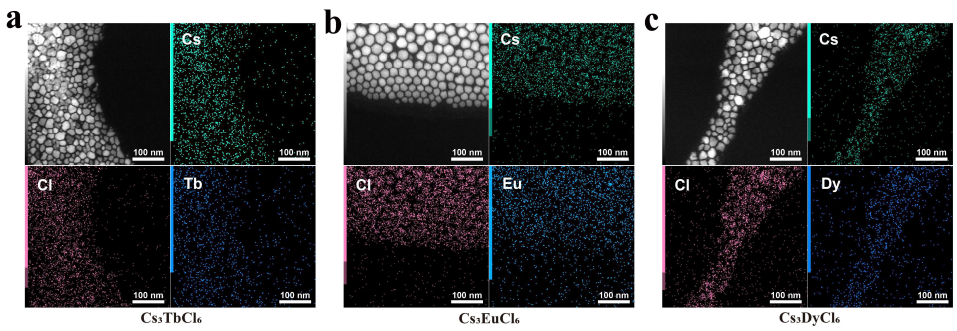

Figure S3. Elemental mapping of (a) Cs_3TbCl_6 NCs, (b) Cs_3EuCl_6 NCs and (c) Cs_3DyCl_6 NCs.

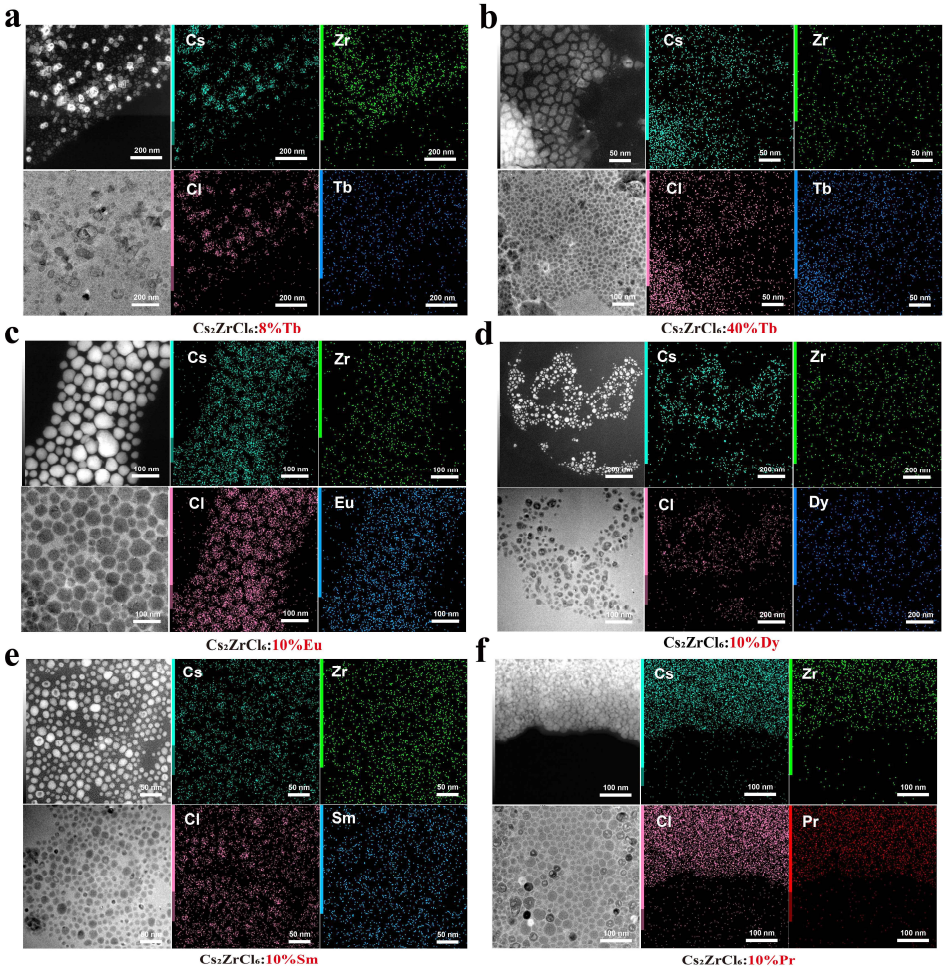

Figure S4. TEM and energy dispersive X-ray mapping analysis for Cs_2ZrCl_6 :xLn^{3+} nanocrystals of different doping ratio. (a) Cs_2ZrCl_6:8%Tb. (b) Cs_2ZrCl_6:40%Tb. (c) Cs_2ZrCl_6:10%Eu. (d) Cs_2ZrCl_6:10%Dy. (e) Cs_2ZrCl_6:10%Sm. (f) Cs_2ZrCl_6:10%Pr.

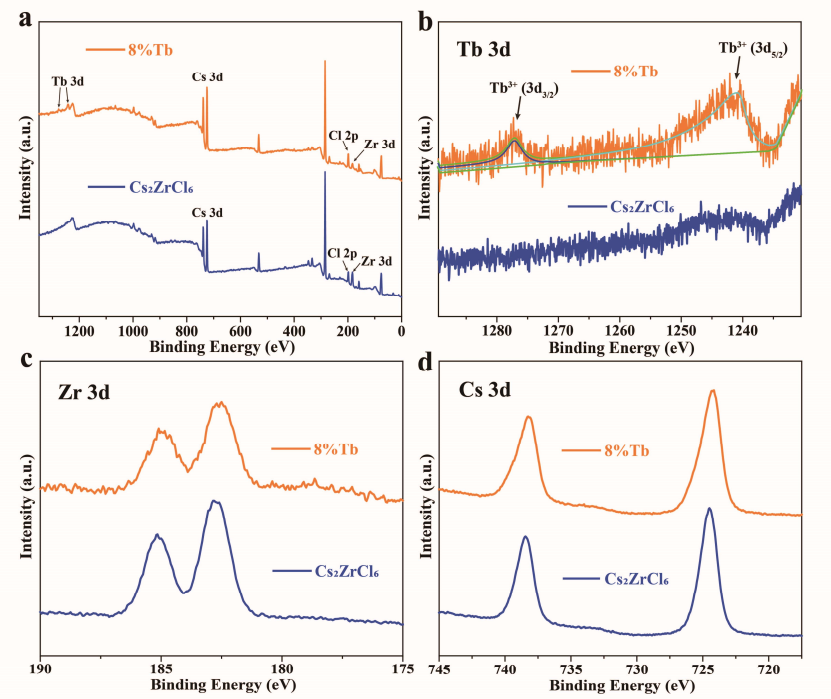

Figure S5. (a) Survey XPS spectra for undoped Cs_2ZrCl_6 NCs and 8%Tb^{3+}-doped Cs_2ZrCl_6 NCs. (b-d) High-resolution XPS spectra of Tb 3d, Zr 3d and Cs 3d, respectively.

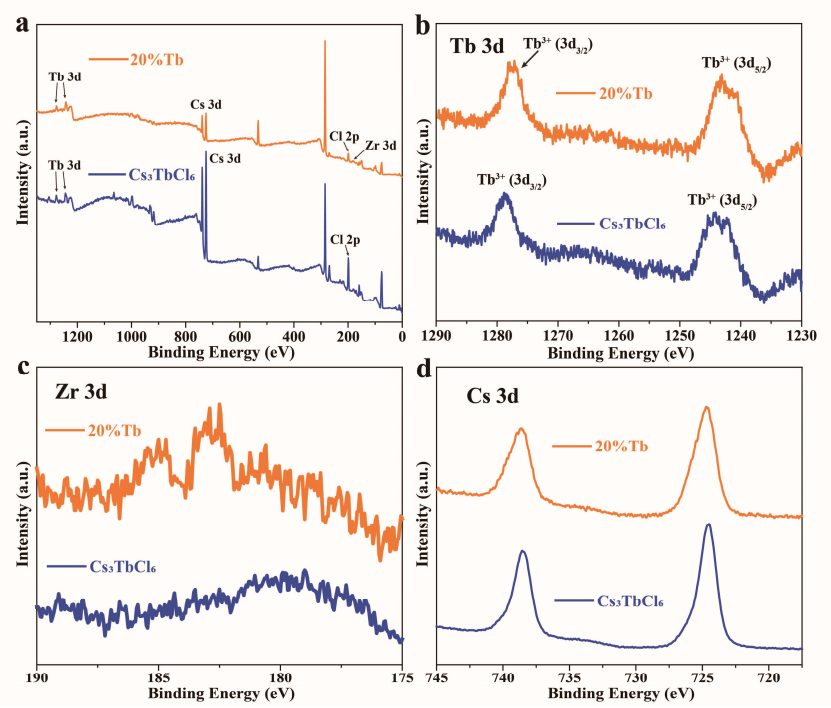

Figure S6. (a) Survey XPS spectra for 20%Tb^{3+}-doped Cs_2ZrCl_6 NCs and undoped Cs_3TbCl_6 NCs. (b-d) High-resolution XPS spectra of Tb 3d, Zr 3d and Cs 3d, respectively.

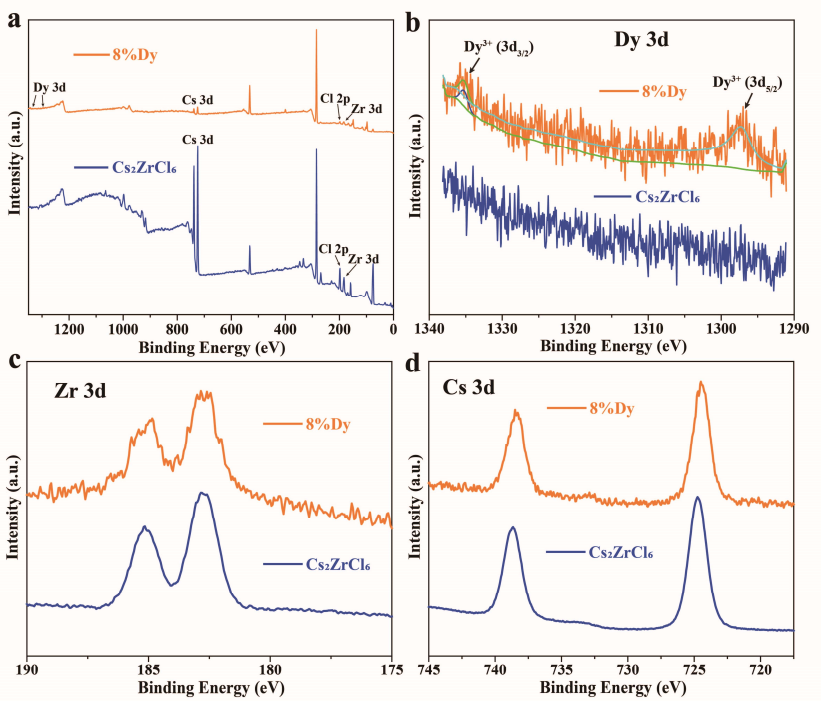

Figure S7. (a) Survey XPS spectra for undoped Cs_2ZrCl_6 NCs and 8%Dy^{3+}-doped Cs_2ZrCl_6 NCs. (b-d) High-resolution XPS spectra of Dy 3d, Zr 3d and Cs 3d, respectively.

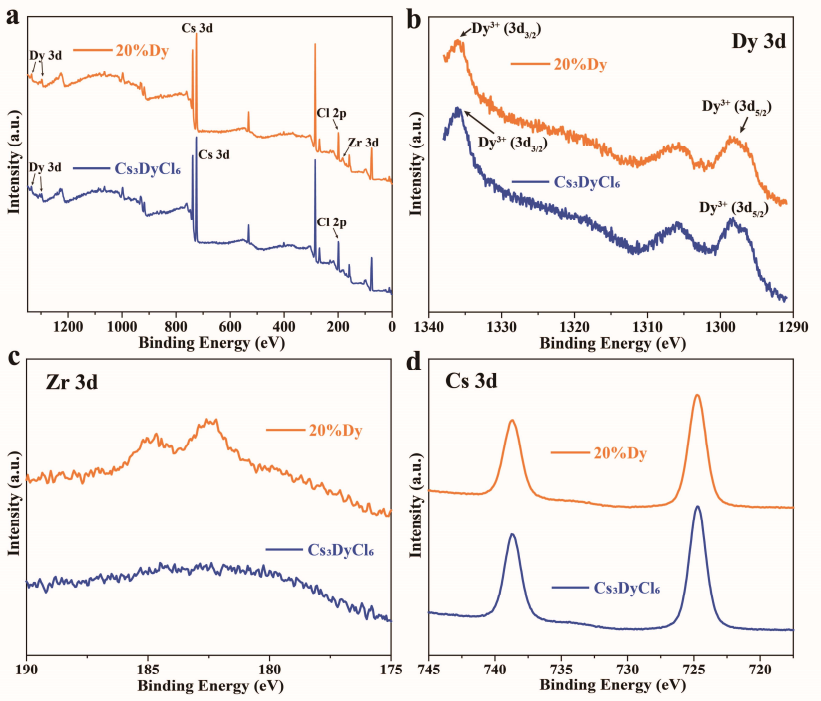

Figure S8. (a) Survey XPS spectra for 20%Dy^{3+}-doped Cs_2ZrCl_6 NCs and undoped Cs_3DyCl_6 NCs. (b-d) High-resolution XPS spectra of Dy 3d, Zr 3d and Cs 3d, respectively.

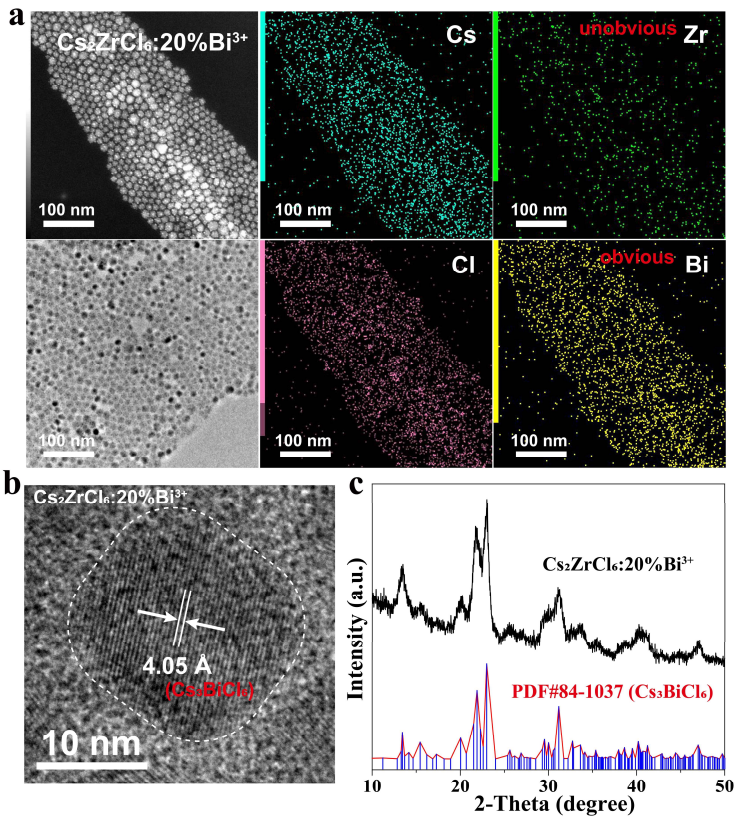

Figure S9. (a) TEM images and energy dispersive X-ray mapping analysis of Cs_2ZrCl_6:20%Bi NCs. (b) HRTEM images of Cs_2ZrCl_6:20%Bi NCs. (c) XRD pattern of Cs_2ZrCl_6:20%Bi NCs.

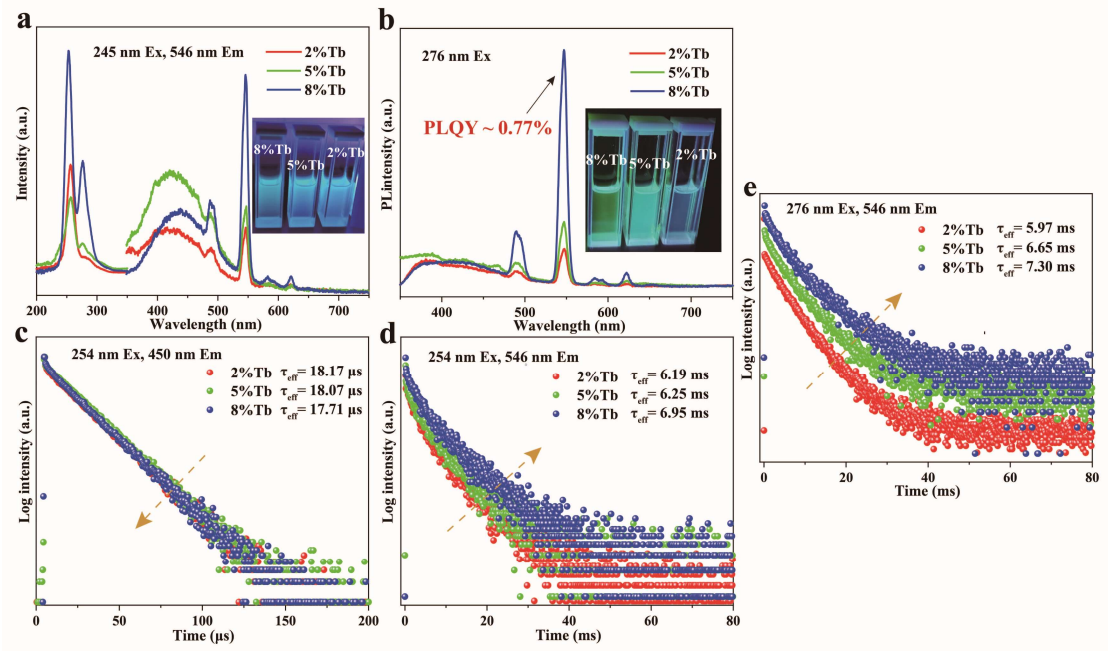

Figure S10. (a) PLE and PL spectra of Cs_2ZrCl_6:xTb NCs (x = 2%, 5%, 8%) under 245 nm excitation and 546 nm emission. (b) PL spectra of Cs_2ZrCl_6:xTb NCs under 276 nm excitation. (c-e) Comparison of PL decay curves of Cs_2ZrCl_6:xTb NCs at 450 nm and 546 nm.

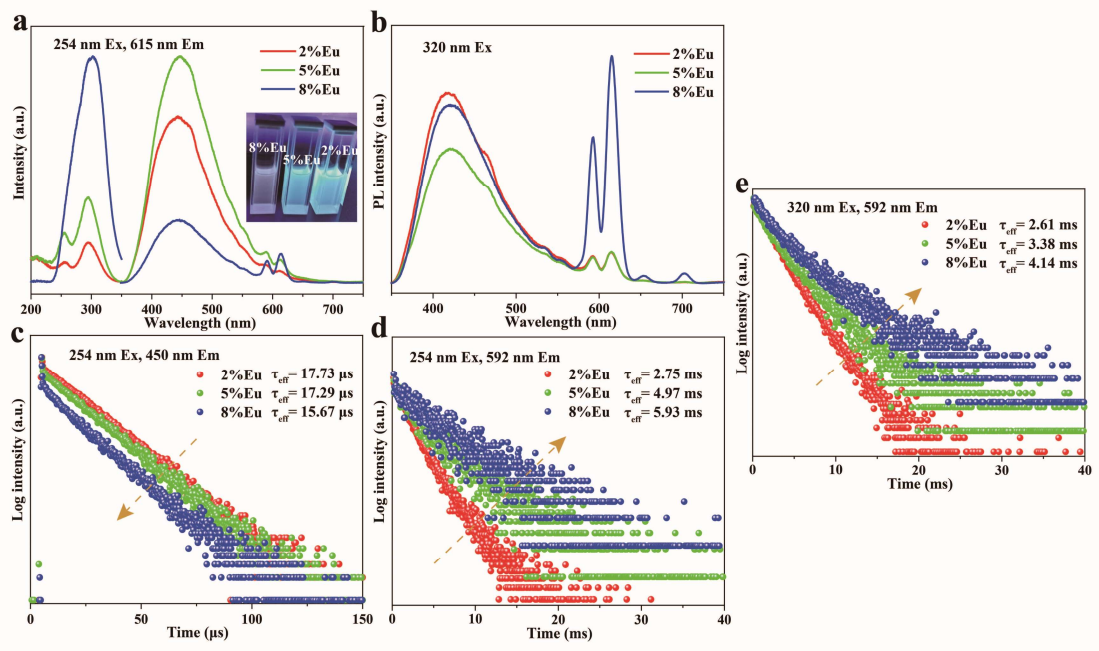

Figure S11. (a) PLE and PL spectra of Cs_2ZrCl_6:xEu NCs (x = 2%, 5%, 8%) under 254 nm excitation and 615 nm emission. (b) PL spectra of Cs_2ZrCl_6:xEu NCs under 320 nm excitation. (c-e) Comparison of PL decay curves of Cs_2ZrCl_6:xEu NCs at 450 nm and 592 nm.

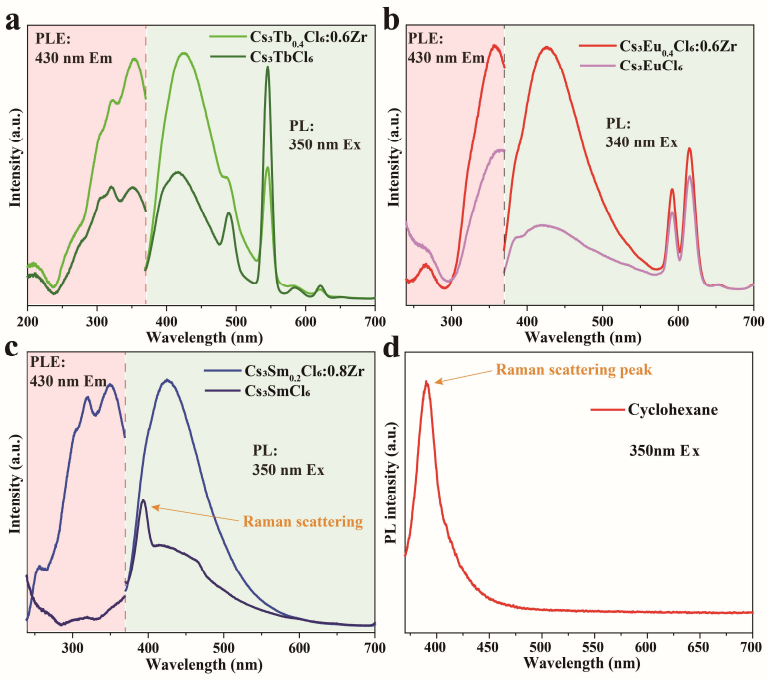

Figure S12. (a) PLE and PL spectra for Cs_3TbCl_6 and $Cs_3Tb_{0.4}Cl_6$:0.6Zr NCs under 350 nm excitation, 430 nm emission. (b) PLE and PL spectra of Cs_3EuCl_6 and $Cs_3Eu_{0.4}Cl_6$:0.6Zr NCs under 340 nm excitation, 430 nm emission. (c) PLE and PL spectra of Cs_3SmCl_6 and $Cs_3Sm_{0.2}Cl_6$:0.8Zr NCs under 350 nm excitation, 430 nm emission. (d) PL spectra of cyclohexane solvent.

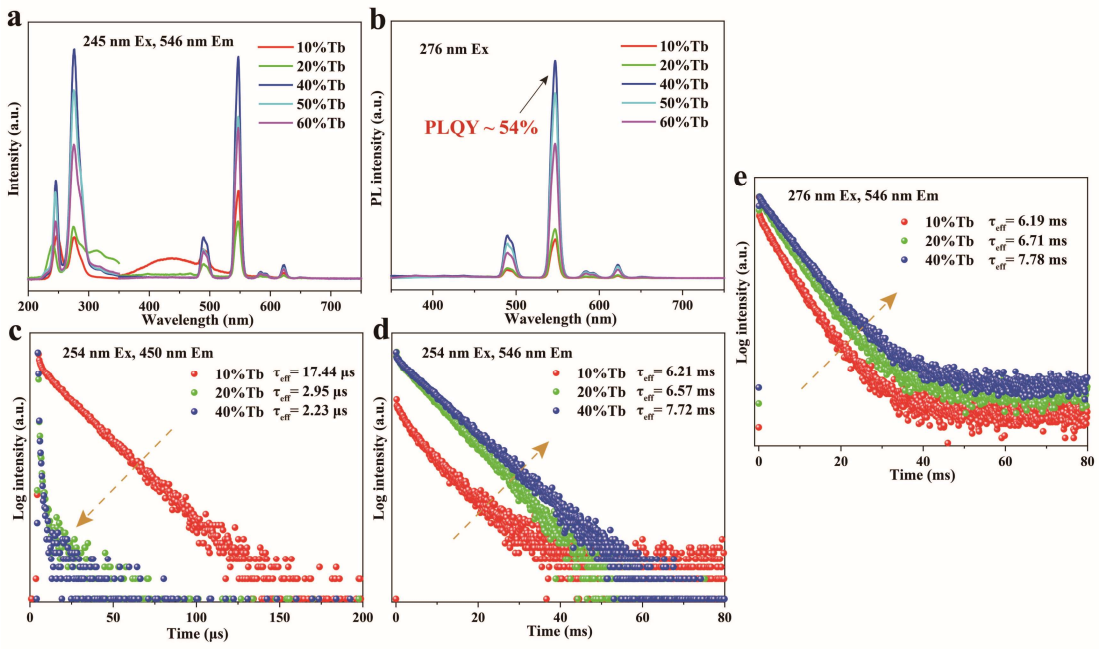

Figure S13. (a) PLE and PL spectra of Cs_2ZrCl_6:xTb NCs (x = 10%, 20%, 40%, 50%, 60%) under 245 nm excitation and 546 nm emission. (b) PL spectra of Cs_2ZrCl_6:xTb NCs under 276 nm excitation. (c-e) Comparison of luminescence decay curves of Cs_2ZrCl_6:xTb NCs at 450 nm and 546 nm.

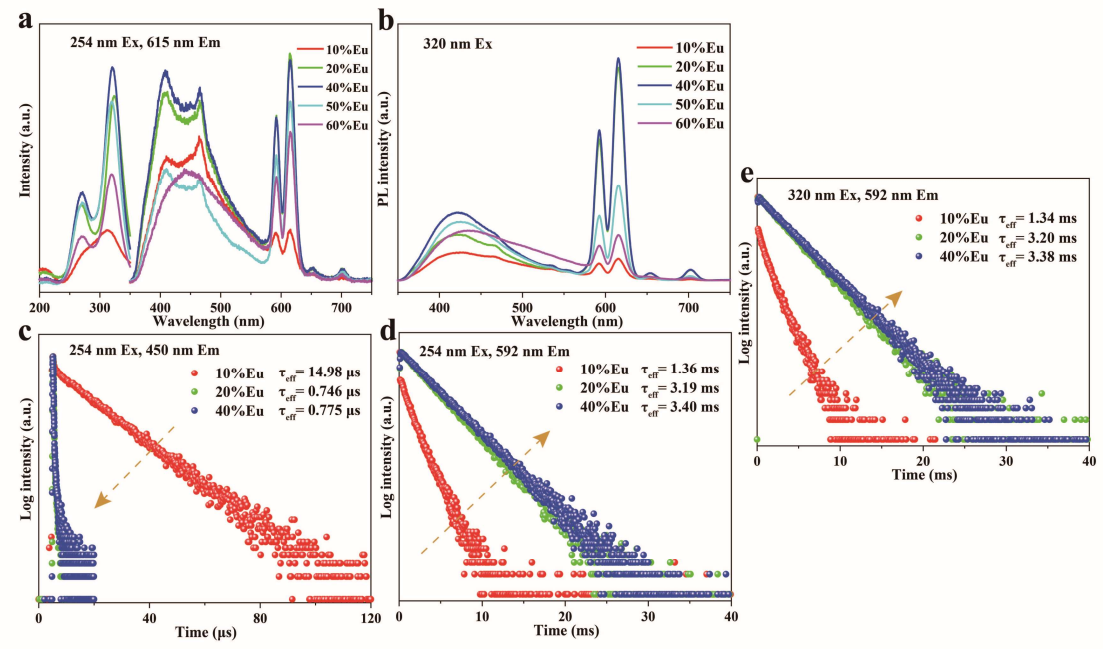

Figure S14. (a) PLE and PL spectra of Cs_2ZrCl_6:xEu NCs (x = 10%, 20%, 40%, 50%, 60%) under 254 nm excitation and 615 nm emission. (b) PL spectra of Cs_2ZrCl_6:xEu NCs under 320 nm excitation. (c-e) Comparison of luminescence decay curves of Cs_2ZrCl_6:xEu NCs at 450 nm and 592 nm.

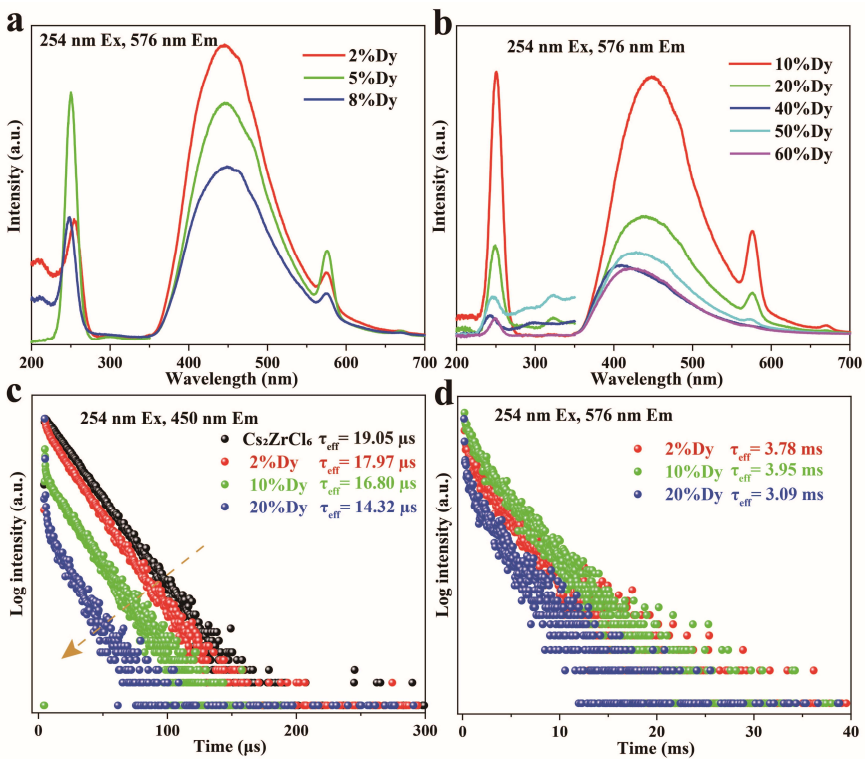

Figure S15. (a-b) PLE and PL spectra of Cs_2ZrCl_6:xDy NCs (x = 2% ~ 60%). (c-d) Luminescence decay curves of Cs_2ZrCl_6:xDy NCs at 450 nm and 576 nm (x = 2%, 10%, 20%).

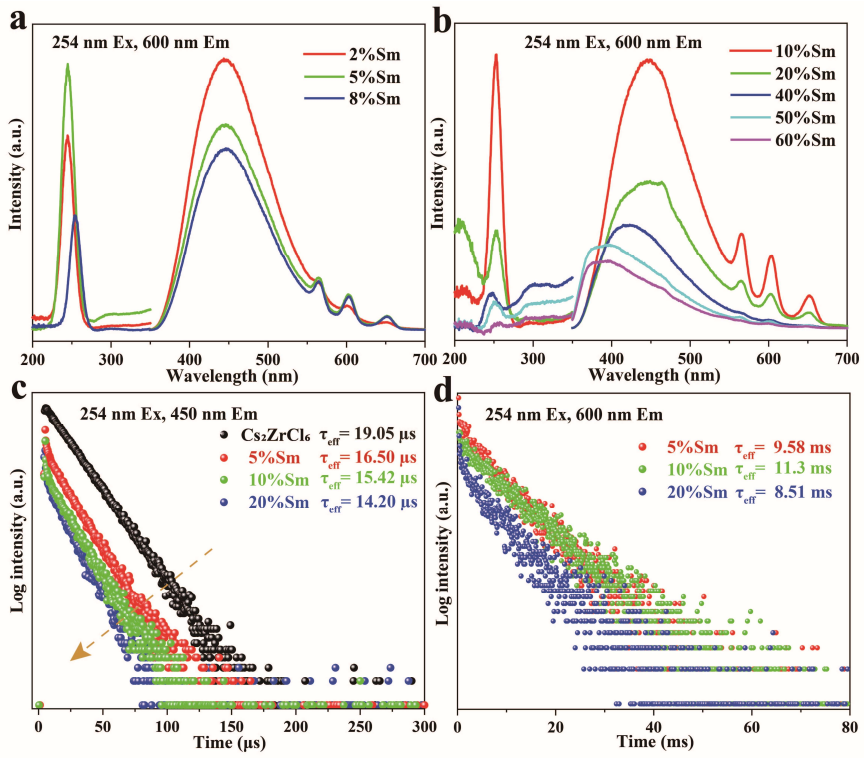

Figure S16. (a-b) PLE and PL spectra of Cs_2ZrCl_6:xSm NCs (x = 2% ~ 60%). (c-d) Luminescence decay curves of Cs_2ZrCl_6:xSm NCs at 450 nm and 600 nm (x = 5%, 10%, 20%).

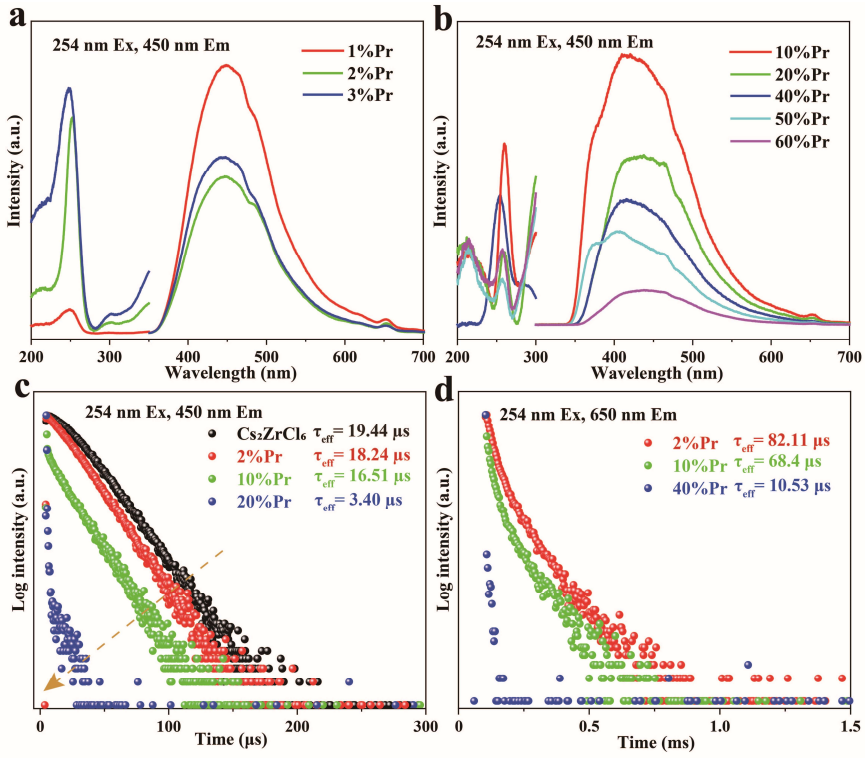

Figure S17. (a-b) PLE and PL spectra of Cs_2ZrCl_6:xPr NCs (x = 1% ~ 60%). (c-d) Luminescence decay curves of Cs_2ZrCl_6:xSm NCs at 450 nm and 650 nm (x = 2%, 10%, 20%/40%).

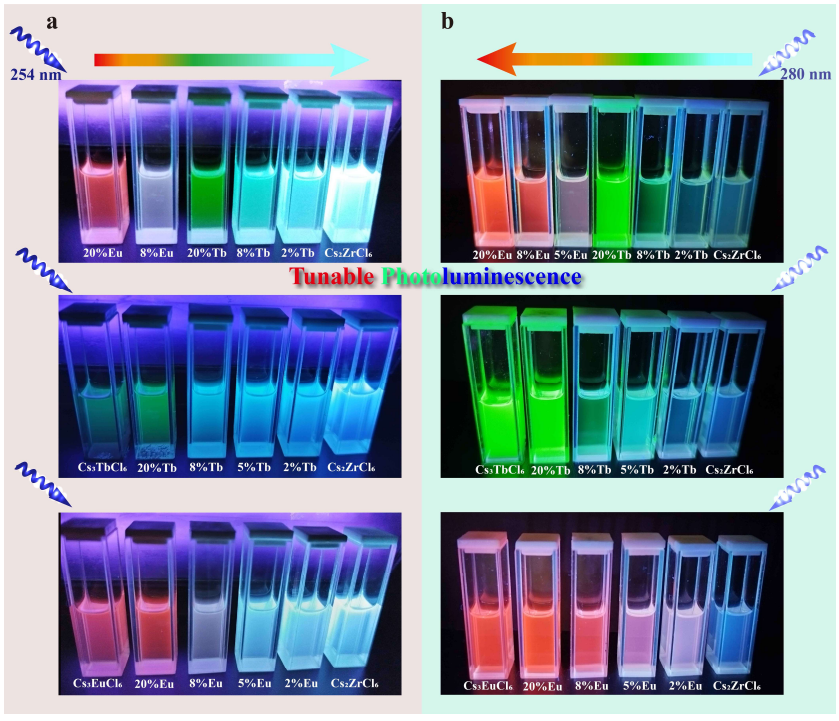

Figure S18. Tunable photoluminescence physical image for Cs_3LnCl_6, undoped and Ln^{3+}-doped Cs_2ZrCl_6 NCs (Ln = Tb^{3+}, Eu^{3+}). (a) Tunable luminescence physical image at 254 nm excitation. (b) Tunable luminescence physical image at 280 nm excitation.

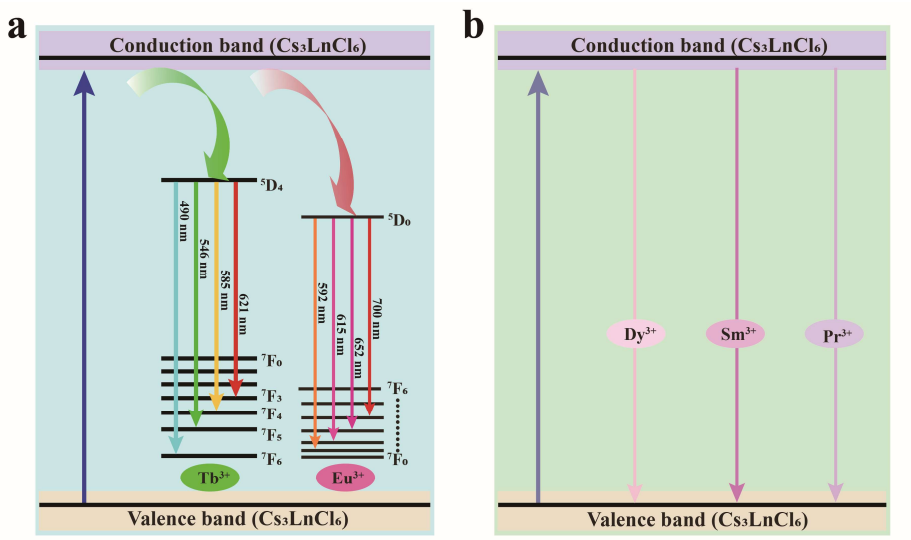

Figure S19. Luminescence mechanism for $Cs_3Ln_xCl_6$:(1-x)Zr^{4+} NCs (x = 100%). (a) Ln = Tb, Eu. (b) Ln = Dy, Sm, Pr.

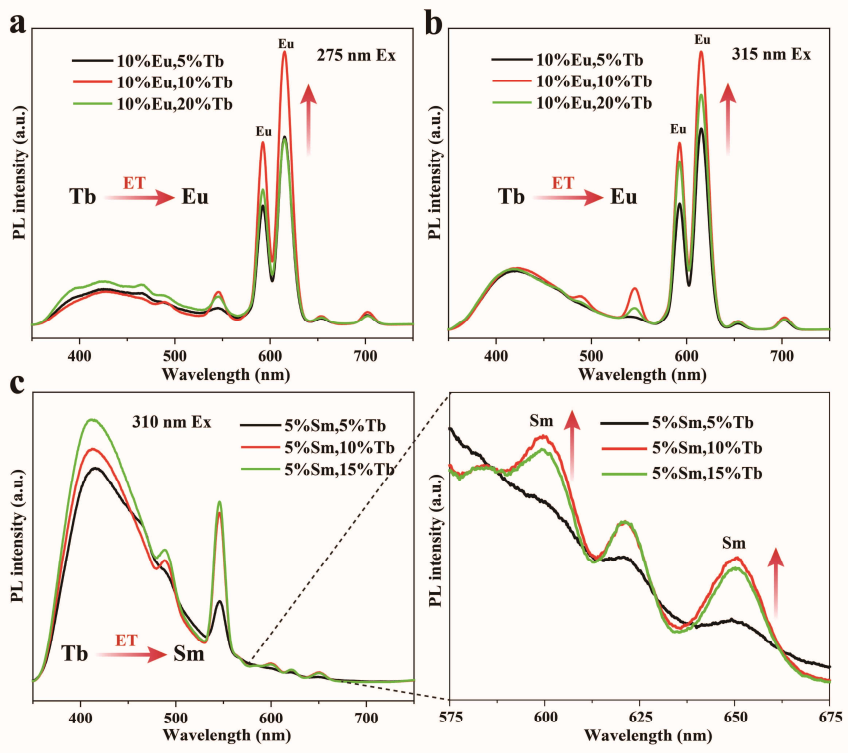

Figure S20. (a-b) PL spectra for Cs_2ZrCl_6:10%Eu, xTb NCs(x = 5%, 10%, 20%) under 275 nm and 315 nm excitation. (c) PL spectra for Cs_2ZrCl_6:5%Sm, xTb NCs(x = 5%, 10%, 15%) under 310 nm excitation (inset: magnification of PL spectra from 575 nm to 675 nm).

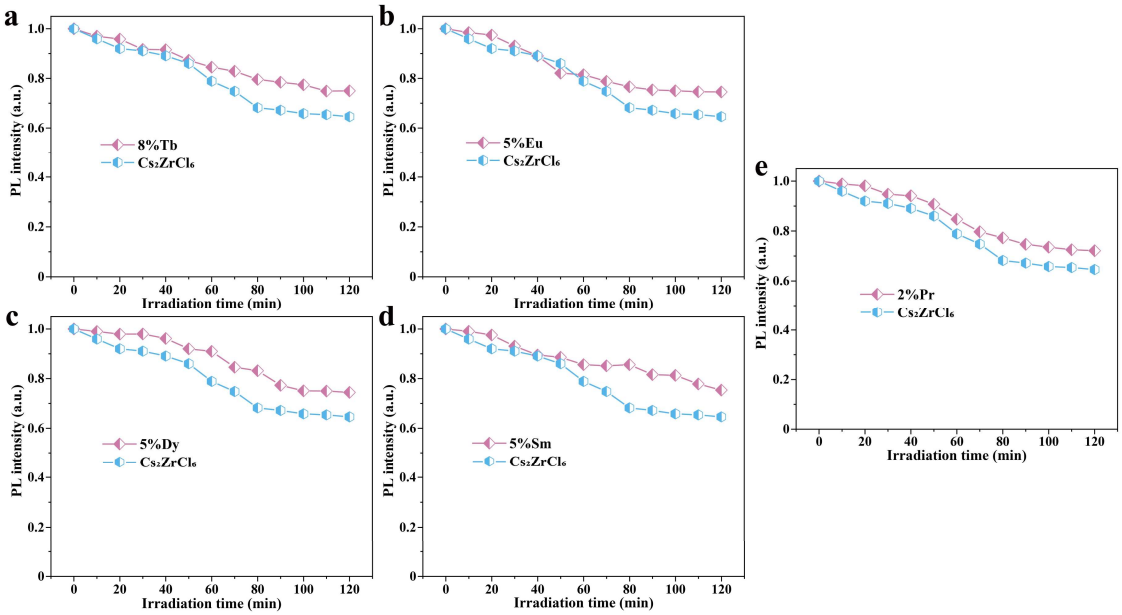

Figure S21. PL intensity change of undoped and Ln^{3+}-doped Cs_2ZrCl_6 NCs (< ~8%, Ln = Tb, Eu, Dy, Sm, Pr) under UV light irradiation (254 nm UV lamp, 20 W). (a) Cs_2ZrCl_6 and Cs_2ZrCl_6:8%Tb. (b) Cs_2ZrCl_6 and Cs_2ZrCl_6:5%Eu. (c) Cs_2ZrCl_6 and Cs_2ZrCl_6:5%Dy. (d) Cs_2ZrCl_6 and Cs_2ZrCl_6:5%Sm. (e) Cs_2ZrCl_6 and Cs_2ZrCl_6:2%Pr.

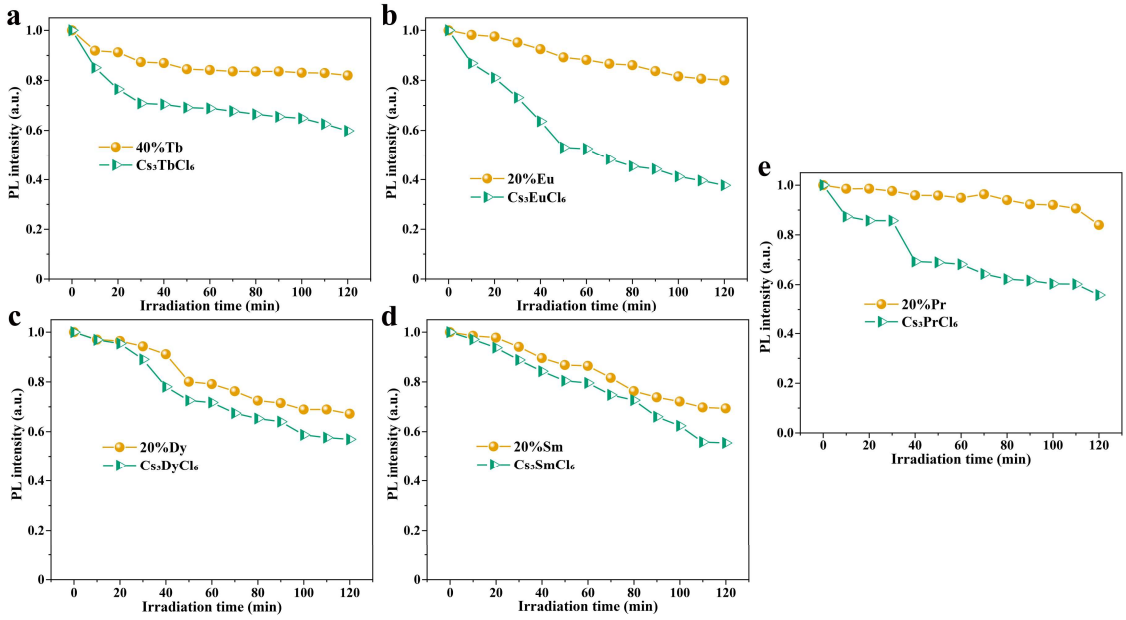

Figure S22. PL intensity change of undoped Cs_3LnCl_6 and Ln^{3+}-doped Cs_2ZrCl_6 NCs (> ~10%, Ln = Tb, Eu, Dy, Sm, Pr) under UV light irradiation (254 nm UV lamp, 20 W). (a) Cs_3TbCl_6 and Cs_2ZrCl_6:40%Tb. (b) Cs_3EuCl_6 and Cs_2ZrCl_6:20%Eu. (c) Cs_3DyCl_6 and Cs_2ZrCl_6:20%Dy. (d) Cs_3SmCl_6 and Cs_2ZrCl_6:20%Sm. (e) Cs_3PrCl_6 and Cs_2ZrCl_6:20%Pr.

References

(1) S. Liu, B. Yang, J. Chen, D. Wei, D. Zheng, Q. Kong, W. Deng and K. Han, *Angew. Chem., Int. Ed.,* 2020, **59**, 21925-21929.

(2) W. Zhou, Y. Yu, P. Han, C. Li, T. Wu, Z. Ding, R. Liu, R. Zhang, C. Luo, H. Li, K. Zhao, K. Han and R. Lu, *Adv. Mater.,* 2024, **36**, 2302140.